TITLE: *Mars Global Surveyor*'s Mars Orbiter Camera (MOC) Wide-Angle Images (1999–2006): 2. Data Investigation into North Polar Hood Formation, Broad Brightness Changes in Acidalia, and Seasonal Frost in Hellas

Stuart J. Robbins*,[a] ORCID: 0000-0002-8585-2549

*stuart@boulder.swri.edu
*Corresponding Author
[a]Southwest Research Institute, 1050 Walnut St., Suite 300, Boulder, CO 80302, United States

Submitted to *Journal of Geophysical Research—Planets*: 27 September 2021
Resubmitted in part to *Journal of Geophysical Research—Planets*: 11 October 2022

Total Pages – 41; Total Tables – 0; Total Figures – 8; Archived Data – NO

Note to Editor(s) and Reviewer(s): This manuscript was originally submitted to *JGR-P* with the data processing methods and observations about Mars in a single manuscript. Reviewers requested some significant revisions and more detail about new observations, so the manuscript was rejected with the invitation to resubmit. After revisiting my processing pipeline, I employed new methods I had developed for processing MARCI data, and I decided that this work should be split in two due to length. The "non-hypothesis-based" first manuscript details how the data were processed and was submitted to *ESS* contemporaneously to this. This second manuscript looks at new science observations with the data processing method excised has been re-submitted to *JGR-P*. I refer in both to the other one as a companion manuscript, despite them being submitted to separate journals (I was instructed that the methods-based one could not go to *JGR-P*). I have also uploaded both, *with* in-manuscript figures, to my personal website (http://www.sjrdesign.net/MOCWA) so that reviewers can see the other one if desired; I have also included the Response to Reviewers in *both* submissions since the original *JGR-P* review contained questions about the data-processing. They are in the preview data directory: http://www.sjrdesign.net/MOCWA

Additional Editorial Note: A few sentences in the second paragraph of this manuscript's Introduction are practically identical to those in the first paragraph of the companion's because that is the best way I could think of to describe the camera/spacecraft.

Publishing Units Count:

Body:

Abstract:	*227 words*	*(250 max)*
§1 Intro:	*573 words*	
§2 Global Observations:	*5,901 words*	
§3 North Polar Hood:	*295 words*	
§4 Acidalia:	*395 words*	
§5 Hellas:	*624 words*	
§6 Discussion:	*257 words*	
Body Σ Words:	8,272 words	
Caption Words:	509 words	*(79+37+44+48+92+82+68+59)*
All Words:	8,781 = 17.562 PU	
Tables:	0 = 0.000 PU	
Figures:	8 = 8.000 PU	
Total:	**= 25.562 PU**	**(SUGGESTED MAX: 25.0)**

Supplemental Material: NO

Archived Data: NO (archived data is part of the "1" paper to *ESS*)

Key Points:

- A new archive of Mars Orbiter Camera Wide-Angle (MOC-WA) images is mined to show several known variations of Mars' surface.
- A new atmospheric study identifying earlier onset of Mars' North Polar Hood formation is demonstrated.
- New studies showing brightness variations in Acidalia and the growth and decline of seasonal frost in Hellas are described.

Plain Language Summary (200-word limit):

The first modern craft to orbit Mars was NASA's *Mars Global Surveyor*, which had the Mars Orbiter Camera. A wide-angle component of that camera took daily global red- and blue-color images during the camera's lifetime, from 1999 through 2006. That dataset has been reprocessed with modern techniques, mosaicked, and grouped into several different time intervals for different types of scientific investigations, and an approximate true-color set of mosaics was also created. Those recently released mosaics reveal a dynamic world of huge cloud systems, changing surface patterns, seasonal changes in frost and ice cover, and vast polar cloud systems as each hemisphere slips into winter. To validate this new work, the reprocessed images are investigated and shown to reveal numerous broad types of surface and atmospheric changes that have been previously demonstrated by other researchers. To show new science that can be done with this work, the data were also examined to study how polar clouds merge together during winter, how the brightness of some features change seasonally, and how frost builds and declines in a vast crater in winter.

Abstract (250-word limit):

Mars Orbiter Camera Wide Angle (MOC-WA) images were taken from late 1999 through most of 2006, in both red and blue, providing nearly daily, nearly global coverage of Mars for approximately four Mars Years. Significant work has been published from those data, but there did not exist a uniform, full time series processing of the data for easier analysis. The companion work to this (Robbins, 202X) presents that processing of the data, producing the full time series in both colors, in equirectangular and polar stereographic projections, in mosaics that have been binned into four different time intervals (daily, $\Delta L_s = 2°$, 5°, and 10° [≈4 through 19 days]) as approximately true-color composites. The multi-dimensional dataset can be mined for surface and atmospheric variations on Mars. To demonstrate basic agreement with past work, several well known trends are demonstrated, including changes after a global dust storm, seasonal frost and ice variations to the poles, and overall surface variations from year-to-year. The data are then analyzed further to demonstrate that the North Polar Hood can form earlier than previously demonstrated, that Acidalia has significant seasonal brightness variations that can be quantified with these data, and the seasonal frost deposition and sublimation of Hellas is quantified. These different investigations represent just a small slice of what can be done now that these data are made available in readily accessible formats.

Keywords: Mars; mosaic; global data; dust; clouds; ice

1. Introduction and Context

A fleet of Mars-observing platforms has provided practically global, continuous coverage of the red planet for more than 23 years, since NASA's *Mars Global Surveyor* (*MGS*) entered orbit in September 1997, and it began to take regular science data nearly two Earth years later. The *MGS*'s primary camera, Mars Orbiter Camera (MOC; Malin et al. 1991), began commissioning images in March 1999, and science images began April 3, 1999. The camera returned images through October 15, 2006. The wide-angle component of MOC (MOC-WA) had a 140° field-of-view which, at its altitude of 373–437 km, meant it could capture pole-to-pole images with nearly continuous longitude coverage over 13 orbits with both its red (575–625 nm) and blue (400–450 nm) cameras. On Mars, red light mostly captures the surface, while blue light is much more sensitive to atmospheric clouds and haze. With an orbital period of 1.95 hours and inclination of 92.5°, the images were taken with an approximately consistent solar illumination of the entire disk, every day (except for when issues arose), for over seven Earth years, corresponding to just over four Mars Years (MY24–28). These images provided nearly daily, global, resolved coverage of Mars from orbit. This dataset presents the only consistent orbital atlas of Mars for this time period, can be mined to better understand how Mars changed during those years, and place those changes in context with what we have learned about Mars throughout the decades.

The companion work to this (Robbins, 202X) presents details of a thorough reprocessing of the MOC-WA image data for those images in spatial summing modes 8, 10, 13, and 27 that returned approximately pole-to-pole-spanning views. In that work, the data were processed with an average photometric correction, had additional empirical flat-fields applied, and were rendered at 9 pix/deg (≈6586 m/pix at the center of the projection). In the archive accompanying that work, the data are presented in many ways: {time averages: daily, $\Delta L_s = 2°$, $\Delta L_s = 5°$, $\Delta L_s = 10°$} × {projections: equirectangular, north polar stereographic, south polar stereographic} × {incidence angle cutoffs: ≤75°, ≤90°} × {color: blue, red, red-(synthetic)green-blue composite}.

Therefore, this large archive not only presents three dimensions of data to be analyzed (spatial, temporal, color), but one can do so using 72 different sets.

There are many published works that use the MOC instrument dataset, though the majority focus on the higher spatial resolution data (*e.g.*, MOC-WA spatial summing mode 1) and those images from the narrow-angle component (MOC-NA). Still, a sizeable body of work has used the global coverage data, though none processed the complete dataset as in the Robbins (202X) companion work, and extremely few make use of the entire time series.

The purpose of this work is to first demonstrate that this reprocessing clearly shows several well-known phenomena on Mars, as a basic quality check, which is discussed in narrative form in section 2. Section 3 begins to use this new archive to perform new science investigations, beginning with the color composites' demonstration that the North Polar Hood can form earlier than previously described. Section 4 performs a new science investigation using the red light component of MOC-WA to quantitatively look at seasonal brightness changes in Acidalia. Section 5 uses the blue mosaics to examine the growth and retreat of frost in Hellas basin, something that has not been described in detail before. Section 6 contains a summary and discussion.

2. Large-Scale Observations of Mars' Changing Surface and Atmosphere

Numerous features are named in this and the next section, and they are labeled in Figure 1. This section is meant to show the broad utility of the dataset for identifying features and their changes, and how these data can be used to show what others have found when also using these or related data, such as the report of James & Cantor (2002) covering roughly the first full Mars Year of MOC-WA data.

2.1. Data Analysis Method: Color Composites

2.1.1. Approximate True Color Composites

For much of the analysis in this and later sections, visual inspection was done on both the greyscale red or blue images as well as on synthetic three-color composites. Due to some cartographic control issues and camera models that could be improved, there is some red-blue fringing, especially visible near the poles in the individual orbits. See Robbins (202X) for additional processing details.

2.1.2. RGB and RC Color Composites to Identify Differences

A second method was used in some circumstances to create false-color composites to help identify changes. The RGB method takes any three images (in the same projection, and from the same filter), and sets one image to red, another to green, and the third to blue; the RC method sets one to red and the other to cyan. The blending mode is "screen" in either case, which is a common method to make these composites (screen for two images with brightnesses a and b in a given pixel location is defined as $f(a,b) = 1-(1-a)\cdot(1-b)$). The effect is that any lighter component from any image becomes apparent so that image's color dominates at that pixel. Therefore, for RGB, if there is a region where the image set to green is brighter, it will appear green in the composite. If there is a region where any two are brighter than the third, it will appear as the additive color of the two: yellow, cyan, or magenta. For the RC method, areas where the two images are the same brightness will be greyscale. (While it is perhaps undesirable for the sum of red/cyan to be greyscale due to the red/blue nature of the cameras' sensitivity, the colors *must* be 180° of hue apart, and they must be quantized in 60° options [*e.g.*, pure red, or pure yellow] for proper rendering in a given colorspace. For best colorblind-safe visibility, red-cyan was selected.) Figure 2 shows these colorscales. This method is useful when visually searching for subtle, smaller changes.

2.2. Global Weather Patterns and Most Persistent Clouds

Before describing observations from this time series, it should be noted that a *substantial* body of work exists that has studied and analyzed the Martian atmosphere and clouds, including the recent book, The Atmosphere and Climate of Mars (Haberle, Clancy, Forget, Smith, and Zurek, eds., 2017). Past work includes everything from Earth-based telescopic observations to space-based telescopic observations, and early Mars flyby craft from *Mariner* through modern missions by a variety of world space agencies. Attempts have been made to cite some of the relevant literature that first identified the features discussed herein using MOC-WA data, while acknowledging that a thorough reference list would number into the hundreds. In particular for this first science subsection, the work of Benson et al. (2003, 2006) involved identification and measurement of clouds around the primary martian volcanoes and western region of the Valles Marineris canyon system over the course of three Mars Years, and they identified many of the trends noted below. The earlier work of Wang & Ingersoll (2002) is another seminal article which describes the phenomena discussed in this section, including the aphelion cloud belt, from one Mars Year of MOC imaging; Cantor et al. (2002) also describe atmospheric phenomena spanning three seasons of northern summer, going back into some of the pre-commissioning data in 1997.

The most persistent and large cloud features visible in the mosaics surround the four tallest Tharsis volcanoes. Clouds can be seen on or around them in practically all mosaics, though they grow and shrink in intensity and occasionally disappear around some. For example, during the southern summer, all but the clouds around the southernmost Arsia Mons disappear, and those around Arsia reach a minimum opacity around $L_s \sim 320$–$340°$. They are significantly diminished around Arsia starting at $L_s \sim 220°$, practically disappearing in MY26 between $L_s =$ 210° to 220°, but they are still very faintly present. Clouds around Elysium Mons are similarly persistent in most mosaics, but being at a slightly more northern latitude than Olympus Mons, clouds around Elysium tend to disappear after the $L_s = 180°$ equinox.

Another persistent cloud formation near a volcano is the lee clouds northeast of Alba Mons, the northernmost of the large Tharsis volcanoes. Lee clouds are seen near it starting $L_s \sim$ 350° and persist until $L_s \sim 220°$. Due to the public interest, it must be noted this is *not* the same as the extremely elongated cloud (~1800 km long, ~10s km wide) sometimes seen from Arsia Mons, most recently described by Hernández-Bernal *et al*. (2021). That cloud occurs near $L_s \sim$ 220–320° (the *opposite* time as the above lee clouds) but is purely a morning phenomenon, starting before sunrise and lasting a few hours. Because MOC-WA imaged consistently in early afternoon, it does not appear in the MOC-WA timeseries.

The clouds surrounding all volcanoes, and cloud cover in general, is most significant near northern summer solstice ($L_s = 90°$). This resolved time series shows they begin to significantly grow in extent and opacity starting $L_s \sim 60°$, and they are significantly diminished by $L_s \sim 140°$, practically symmetric about the solstice.

Beyond the clouds surrounding the volcanoes, another distinct, seasonal feature is an equatorial cloud belt that rises to prominence between the two equinoxes that bracket northern summer, described in some work as the "aphelion cloud belt" (beginning with Clancy *et al*., 1996), given that Mars' aphelion is $L_s \approx 71°$. In Mars Years 26–27, hints of its formation began as early as $L_s \sim 30°$, but it was apparent in MY 25–28 by $L_s \sim 50°$. It is most prominent between approximately –10°N to +30°N, and it dissipates by $L_s \sim 200°$.

Finally, a prominent, repeating cloud feature is the north polar hood, a band of clouds that covers the north pole. While the south polar hood is also well known, it is significantly smaller in extent than the north polar hood, and only prominent in the $i \leq 90°$ mosaics. Both of these are discussed in later sections.

2.3. Effects of Dust Storms

While there were plenty of atmospheric phenomena, including localized dust storms in MY24–28, the primary dust storm of the *MGS* mission occurred in MY25 (late 2001). The 2001 global dust storm has been studied by numerous researchers, with perhaps the primary work cited being Cantor (2007), who detailed MOC observations of the storm as it grew, covered Mars, and eventually dissipated. Another important article that placed the dust storm in context with later ones is by Wang & Richardson (2015), who used daily maps from MOC-WA and MARCI to track not only the global storms from 2001 and 2007, but 63 other large dust storms during 1999–2011.

In this work, the focus is on changes before versus after the storm. The $\Delta L_s = 10°$

timeseries shows that $L_s = 180°$ in MY25 is practically identical to MY24 and MY26, but by $L_s = 190°$, surface features were substantially obscured. For $L_s = 210°$, all that is apparent is a darker mid- to high-northern latitude band, the frost line in the southern hemisphere, the tops of the tallest Tharsis volcanoes (indicating the vertical extent of the dust storm did not create an optically thick atmosphere at +15 km), and very dark features along the southern margins of Tharsis and Elysium. This is a case where the $\Delta L_s = 10°$ can give a false impression: Looking at finer time-scale mosaics, various other surface features are visible at any given time, often covered with optically thin dust clouds, but the rapidly moving, optically thick dust obscures those features in the longer time averages. The individual orbit mosaics show large amounts of dust clouds as early as orbit 10,215 ($L_s = 181°$), but they are transient and localized. By orbit 10,278 ($L_s = 184°$), large dust cloud fronts covering thousands of kilometers are visible, which rapidly spread across Mars (illustrated well in Cantor, 2007, so not shown here).

Figure 3 shows an RC composite for $L_s = 180°$ vs 270° for both red and blue; many of the changes observed were discussed in Cantor (2007), but this type of analysis makes many of those changes more obvious, and they did not discuss blue reflectivity changes. Besides the seasonal southern frost showing prominently as red in both panels, and clouds near the Tharsis volcanos as deep red in the bottom (blue camera) panel, there are substantial changes across Mars that cannot easily be correlated with topography, specific geology, nor geographic province. For example, in red light, the outskirts of Olympus Mons were brighter before the storm, the mid-flanks were brighter after, and the caldera brighter before. Overall, Mars was brighter in red light after the storm, indicating a veneer of dust deposition covering darker material (assuming proper camera calibration). This is especially true throughout Syrtis Major, and the dark regions of the North/South dichotomy boundary receded several hundred kilometers after the storm, though Terra Meridiani is an exception in that it was brighter in red light before. The western-most region of Noctus Labyrinthus (western Syria Planum) has a bright cyan area hugging it that changes to a broader red area in Figure 3A, indicating a significant change to be brighter after the dust storm right next to the canyon, versus much brighter before the storm to the southeast.

In blue light, the differences are more muted, though this could be due to the lower signal-to-noise. However, the same trend seen in red light appears for Olympus and Elysium Montes, while most of the southern hemisphere appears brighter in blue light after the dust storm. There is a line of red connecting the three Elysium Planitia volcanoes that then arcs around the Elysium Mons flank, indicating this area was brighter before than after, but this could is likely due to clouds that dissipated sometime between equinox and southern summer. Tharsis in general was brighter before than after, as was most of the surface surrounding Valles Marineris, but both are likely due to the aphelion cloud belt dissipating. Interestingly, Valles Marineris stands out clearly in Figure 3B as a neutral color, indicating it was approximately the same brightness before and after the storm.

2.4. North Polar Phenomena

North polar phenomena observed with MOC (and MARCI) are reviewed in a large part by Cantor et al. (2010) who combined MOC-WA and MARCI data, and this work tends to reproduce many of their observations. Additionally, Calvin *et al*. (2015) provides a good overview of the surface features observed here with MOC-WA, but identified in subsequent years with MARCI. As with section 2.2, Wang & Ingersoll (2002) also have a good overview of the atmospheric observations discussed here, but their work only covers the first Mars Year of MOC's operation.

2.4.1. North Polar Hood (Cloud Cover)

The north polar hood (NPH) has been known since the era of telescopic observations and was studied from the first orbital photography as far back as *Mariner 9* (Briggs & Leovy, 1974). Due to various factors including topography and Mars' eccentric orbit, the NPH is significantly more extensive and longer-lasting than the corresponding south polar hood. Wang and Ingersoll (2002), who studied the first year of MOC-WA data, found the NPH forms during $L_s \sim 160°$–$185°$; this was replicated in Calvin et al. (2015) who found in MY29 and 30 that it formed at $L_s \sim 158°$. Similar results are found here for each MOC-WA-covered Mars Year, except MY27 when the hood began to form as early as $L_s \sim 140°$ (discussed in section 3). It is still optically thin in $L_s \sim 170°$ mosaics, but by $L_s = 180°$, the hood is opaque in every Mars Year covered by these data. The hood persists through southern summer and the following equinox, dissipating by $L_s \sim 40°$, meaning it persists across ~200° of Mars' orbit.

2.4.2. Seasonal Frost Deposition and Retreat to the Residual Ice Cap

Substantial work could be done analyzing polar frost deposits and the residual cap from these mosaics, and some work with these data has been done by James & Cantor (2001), Benson & James (2003), Calvin *et al*. (2015), though the latter relied mostly on MARCI data; earlier work spanned telescopic observations (*e.g.*, Herschel, 1784, Slipher, 1962, Iwasaki et al., 1979, 1982, 1984, 199, Cantor, 1998) and early spacecraft observations (*e.g.*, Soderblom et al., 1973, James, 1979, 1982). In the interest of space, a basic analysis of extent and yearly differences are presented here. In general, the seasonal water and CO_2 cycle – of which the NPH is a component – deposits a circular region of surface frost that extends almost as far south as the NPH's extent, to roughly the latitude of Lyot crater (~+50°N). As the region transitions to summer, the roughly circular frost line retreats towards the residual cap in a mostly repeatable, fairly linear pattern from year-to-year (*e.g.*, Benson & James, 2003). By the summer solstice, all of the seasonal frost disappears, leaving the residual cap. The residual cap remains stable (at MOC-WA scales) until it fades from view under the NPH and winter night.

Despite remaining relatively static past the solstice, the residual cap is still revealed as a dynamic feature in these data, which are presented here in a novel way: Figure 4 illustrates in the top row an RGB composite as the season progresses past summer solstice for MY25, 26, and 27. The ice does not significantly retreat further after the solstice. However, there are substantial brightness variations across the cap. Starting at lower latitudes, the detached ice roughly symmetric about the antemeridian appears bluer, indicating it is brighter near $L_s = 130°$ than at $L_s = 90°$ or 110°. On the cap, as one approaches the north pole, the colors shift along the rainbow from blue to red, indicating progressive brightening along lower latitudes as the season progresses, and darkening towards the middle as the season progresses. There are small areas of saturated red in the troughs, indicating some minor ice retreat (at MOC-WA scales) after the solstice. The ice cap is bluer at the southern-most extent over longitudes ~0–90°, indicating brightening of some form at L_s ~ 40° past the solstice, possibly from dust being removed to reveal the brighter ice, or simply deposition of CO_2 and H_2O frost (Byrne et al., 2008).

The cap also shows secular variations from year-to-year, illustrated in Figure 5 with the splashes of color throughout, indicating differing ice extent in different locations per year, with no apparent pattern.

2.4.3. Variations Near the Cap (North of ≈60°N)

Examining the full time series color mosaics, relatively little in the north changes from year-to-year that has not been already discussed. While there appear to be some overall color and possibly some contrast changes, these cannot be ruled out as instrument fluctuations. What is likely not an instrument fluctuation is that the north polar cap appears to darken in its center starting L_s ~ 130°. It is possible that this is unaccounted for limb darkening or atmospheric scattering, but that is unlikely given the $i \leq 75°$ clip, and that cutoff does not begin to exclude polar pixels until L_s ~ 150°; this type of darkening was also observed by Byrne *et al*. (2008) using the Mars Orbiter Laser Altimeter as a passive radiometer, and they attributed the darkening to topographic shading. Turning to Figure 4 to try to discern more subtle changes, there are large, cohesive blobs of color surrounding the pole in each Mars Year that are not the same (though they are similar in MY26 and MY27). This indicates that as summer turns to autumn, there are brightness differences that are not symmetric about the pole. However, any particular pattern is not obvious. It is possible that this signals the beginnings of highly variable clouds as the season progresses that will eventually form the polar hood, or sub-pixel-scale topographic shading, but that is not clear in these data. Figure 5 shows similar large splotches of color surrounding the poles at L_s = 90°, indicating brighter material in MY26 and MY28 near Acidalia, but the yellow elsewhere indicates brighter material near MY26 and MY27 elsewhere.

2.5. South Polar Phenomena

South polar phenomena observed with MOC-WA do not have a general manuscript similar to Cantor et al. (2010) for the north. Calvin *et al*. (2017) provide a good overview of the surface features observed here with MOC-WA, but identified in subsequent years with MARCI.

2.5.1. South Polar Hood (Cloud Cover)

The south polar hood (SPH) is formed the same way as the north, from a series of storms that merge as the season changes from southern summer to autumnal equinox. Wang and Ingersoll (2002) characterize the start near $L_s \sim 340°$, and there is continued growth through the winter. While this phenomenon is more clear in daily mosaics, in any of the ΔL_s time-averaged mosaics here, the SPH is *much* less obvious than the NPH. This is because it is significantly more optically thin, something that has been known for many years (*e.g.*, Clancy *et al*., 2017, and references therein). Also apparent is that the south pole appears to darken around L_s ~290°, but this seems to be a surface phenomenon rather than atmospheric because the residual cap retains its brightness as it shrinks (see next sub-section); Byrne *et al*. (2008) also note that the brightness of the cap itself is fairly stable until later in the season when it darkens, again attributed to topographic shading at the <80 cm relief level.

Cloud formation is not obvious until almost the equinox, at which point features lose contrast in a way that can be attributed to atmospheric obscuration. Clouds and haze are more apparent after the $L_s = 0°$ equinox, but they are close to the terminator and therefore hard to identify in the $i \leq 75°$ mosaics; they are slightly more apparent in the $i \leq 90°$ mosaics, and they are significantly more apparent in daily mosaics – something that Wang et al. (2011) tracked over the course of the full time series. Clouds and haze are most prominent near $L_s \approx 10–20°$, extending as far north as southern Argyre and Galle crater (~–50°N). Additionally, there is significantly more frost cover around the south pole during its winter than the north, such that differentiating between atmospheric clouds and ground ice is more difficult with just these images. (The more extensive frost is due to colder temperatures since Mars is near aphelion during southern winter.) Based on coloration of the south polar cap region, assuming the hood is more orange than white in these composites, it appears as though the clouds mostly dissipate by $L_s \sim 230°$. If this color can be a reliable indicator, it is a similar L_s duration as the NPH.

2.5.2. Seasonal Frost Deposition and Retreat to the Residual Ice Cap

James et al. (2001) provide a detailed analysis of the cap's recession and brightness based on one year of MOC-WA data (1999–2000), similar to their 1979 work (James et al., 1979), while the purpose here is to show similar – if more abridged – trends when looking at the entire MOC-WA timeseries. As in the north, seasonal frost is deposited during south polar night and twilight that extends north to Galle (~–50°N). Due to the substantial topographic roughness in the southern hemisphere, in contrast with the northern, the seasonal frost extends into crater floors at a given latitude before the surrounding terrain, typically beginning at the northern walls and floors of those craters since they receive less direct sun. Starting $L_s \sim 50°$, both Hells and Argyre begin to fill with ice, as well; the ice in northern Hellas (present by $L_s \sim 90°$) is the northern-most extent of the seasonal frost, and it persists there until $L_s \sim 140°$, disappearing from most of Hellas within just a few weeks (see section 5). The retreat from the mid-latitudes is very consistent across Mars Years.

Due to topography variations, by $L_s \sim 180°$, the circular frost around the pole becomes more hexagonal. At $L_s \sim 230°$, the ice's outline takes a much less regular shape. Part of this is due to the ice on the Mountains of Mitchel (Mitchel, 1846) that extends beyond the defosting pole by $L_s = 230°$, and the mountains' ices fully detach from the retreating cap between $L_s = 260$–$270°$. As noted in Bonev *et al*. (2002), but extended here another two Mars Years, the Mountains of Mitchel have highly variable frost cover from year-to-year during southern summer at a given L_s, even at MOC-WA resolution; this is partly illustrated in the bottom panel of Figure 5, which shows the mountains as white in just a few pixels in the middle (same ice cover across years), yellow-orange west of that (more ice in MY24 and 26), and red east of that (more ice in MY24). The seasonal frost in these images is always less bright than the residual cap.

As noted for decades, the south residual cap is much smaller than the north's. As shown in Figure 4, it continues to shrink well after the southern solstice, again in contrast with the north's. Familiar dark troughs within the ice do not appear until L_s ~ 300°. Figure 4 is otherwise uninformative with respect to periodic or secular changes within ~30° latitude of the pole, unlike for the north residual cap. Returning to Figure 5, besides the above-discussed Mountains of Mitchel, the ice cap at L_s = 270° across three Mars Years shows substantial variation, as the north cap did and as Calvin *et al*. (2017) demonstrated with MARCI data. In interpreting this, it must be first recognized that roughly half of the ice extent at the south pole during the summer solstice is still seasonal frost, unlike the north. With that in mind, the most substantial secular differences are seen in this seasonal frost region, stretching from ~210°E, clockwise in the Figure, to ~30°E. The coloration in Figure 5 appears as a mottling of mostly yellow and green, indicating more ice extent in both MY26 and the combination of MY24 and 26. Opposite and much closer to the residual cap, the ice fringes appear blue and purple, indicating more ice extent in those areas in both MY24 and 27, in contrast to MY26.

2.5.3. Variations Near the Cap (South of ≈60°S)

In contrast with the north, the south polar cap in the color mosaics appears to show some drastic brightness and color changes that are not attributable to a capricious instrument. After passing through summer solstice, beginning just outside the ice cap and spreading out from there as L_s increases, the surface appears both darker and redder. This is not an instrument issue and probably not topographic shading because it varies across Mars Years in intensity and has a highly limited latitude range. Figure 4 helps illustrate this, showing that in MY24 and MY25, there is a yellow region surrounding the ice, indicating that it is much brighter in that area in red light during L_s = 300–310° than at 320°. However, this is significantly muted in MY26, and it is a blue ring in MY27 that indicates it is brighter in that area later in the season during that year. The polar darkening persists until L_s ~ 150°, over half of Mars' year. It is also more red in this time, though it is possible that there is an undescribed systematic issue with the blue vs red MOC-WA gain.

2.6. Solis Planum

Solis Planum (or Lacus in some works, despite the official IAU "Planum" designation), approximately centered at ~20°S, ~85°W, is a 2.6 million km^2 region forming the southeast portion of the Tharsis rise. Topographically, it is relatively flat, gently sloping southeast from the topographic high at the western end of Valles Marineris. It is bound to the north by Valles Marineris, and it is bound on all other sides by a nearly continuous set of ridges and mountains. Conceptually, one might think of the entire region as a large sand trap, the mountains helping to focus and contain material and setting up rebound effects if material cannot be lofted high enough to escape the region. The only "out" is Valles Marineris, but global circulation models indicate that, most frequently, winds flow southeast in the region, so Valles Marineris would not be a common escape route (Forget *et al*., 1999; Millour *et al*., 2018).

With that context, Solis Planum has been known for over a century as the "Eye of Mars," so-called because of a somewhat common lenticular dark dust formation centered in an otherwise lighter region, but it is a feature that frequently changes its appearance. Work from the MOC-WA time sequence suggests this moniker and reputation is well earned, for it was one of the most frequently changing regions observed (*e.g.*, Figure 6, which is described in detail in section 2.9). Relatively little has been published on the topic of surface changes in modern peer-reviewed literature, with most in the form of conference abstracts for the last several decades, mostly based on *Viking* data (Huguenin, 1979; Mouginis-Mark et al., 1980; Lee, 1986) but one more recently based on HiRISE (Geissler & The HiRISE Team, 2012). Additionally, numerous reports in the *Memoirs of the British Astronomical Association* describe it as a changing feature, at least back to 1896 and at least as late as 1927.

While the MOC-WA time series itself shows changes, practically all of the other composites also demonstrate this variability. Figure 3 shows that the northern half of Solis

Planum was much brighter before the global dust storm in MY25 than after, and the southern half brighter after than before. The bottom row of Figure 4 shows that in MY26, it was brighter towards the north for L_s = 300–310°, and significantly brighter over a larger area to the south just a few weeks later at L_s = 320°. In MY27, it was significantly brighter in the center for L_s = 310°, but the dark lane's periphery was brighter for L_s = 300–310°. In all four years, after southern summer, the brighter area was a relatively constant reflectivity. The composite in Figure 5 and series in Figure 6 show substantial changes across its surface during the four Mars Years observed by MOC-WA, though at a broad scale (100s km), the brightness differences were relatively stable *during* each Mars Year (the splotches of color remain fairly constant in each column). This description indicates both annual and secular changes with no real discernable pattern.

2.7. Syrtis Major

Syrtis Major is a relatively young topographic rise, centered at ~8°N ~68°E, and covering over 1.1 million km^2. It is between the lower elevation Arabia Terra to the west and north, Isidis crater to the east, and Hellas crater to the south. It has two volcanic centers – Nili and Meroe Paterae – which form a linked depression in the middle of the topographic high. Conceptually, as a relative high, one might think that it would be devoid of dust that would preferentially settle in the nearby Isidis basin to the east. However, general circulation models (GCMs) indicate that the complicated regional topography tends to focus dust there from neighboring regions, shearing material from the north, but bringing it in from Isidis to the east, while nearby areas form an almost cyclonic pattern of air circulating throughout the area (Forget *et al.*, 1999; Millour *et al.*, 2018; Read *et al.*, 1997).

As with Solis Planum, Syrtis Major showed a substantial change after the 2001 global dust storm, where the dark material that had dominated a wide area shrank to just a few core regions, meaning the entire area brightened substantially (except the perimeter; also described in Cantor (2007)). Figure 6 shows variation not only with Mars Year at a given L_s, but the splotches of color that indicate brighter material present that year will shift, disappear, or appear for a given L_s. That indicates Syrtis Major's brightness shifts differently, at different times in the year, in a non-repeatable manner. It is important to demonstrate in this dataset for credibility that known trends are visible, and these sorts of variations in Syrtis Major have been described before. For example, as with Solis Planum, *Memoirs of the British Astronomical Association* contains reports of Syrtis Major from at least 1895 to 1927; the *Annals of the Lowell Observatory* include reports from at least 1896 to 1905, and *Popular Astronomy* published reports by Slipher in 1921 and Hamilton that same year. One of the first modern peer-reviewed works was by O'Leary & Jackel (1970), but even after that, most work focusing on Syrtis Major as a rapidly changing albedo pattern are relegated to conference abstracts (e.g., Thompson, 1972; Lee, 1986; and Zinzi, 2006).

2.8. Valles Marineris

Valles Marineris is the largest canyon system in the solar system, spanning >4,000 km in length. It begins with the large feature, Noctis Labyrinthes, one of the highest points on Mars that is not an identified volcanic center. Noctis Labyrinthes broadens into the better-known features of Valles Marineris, which reaches a maximum depth of 7 km and width of 200 km. Valles Marineris begins as a tectonic feature but appears much more fluvially modified as it travels East, appearing to outlet into Chryse Planitia. Due to its substantial depth, one would expect it to act as a sand trap, retaining dust brought in from surrounding regions. However, due to the complicated interplay between it and the nearby Tharsis region on which it originates, it has a much more complex and variable appearance in the MOC-WA time series.

First, Syria Planum, the small, dark feature that is just east of the westernmost portion of Noctis Labyrinthes, changes in brightness throughout the time series. While the coloration in Figure 6 might appear at first to remain stable in each column, there are shifts with L_s, indicating that the variations are not wholly secular. This can also be seen in the bottom panel of Figure 5, though over the short term of a single Mars Year, it can appear quite stable (Figure 4).

Following along the feature towards the east, there is relatively little that changes in Figures 5 and 6, though there are numerous variations along the dark, wind-blown region at the southern rim. This would indicate that variations within Valles Marineris tend to repeat annually. Looking to the bottom row of Figure 4 as an exemplar of variation over the course of several weeks shows that it is dynamic on timescales of weeks, especially towards the east. One of the largest areas of the canyon, Capri Chasma and Eos Chasma, along with Ganges Chasma to the north before it joins the main valley, appear distinctly variegated in the three-color composites of Figure 4. The chasmata are green/cyan/blue/purple, indicating that in different years, the different areas tend to be brighter later in the season rather than earlier (for this narrow L_s slice in Figure 4). MY25 shows the least amount of variation, while MY26 and MY27 show the most, with the variations travelling throughout most of the Valley back along Coprates and Melas chasmata. But, they are also different, where during MY26 the floor is brighter in L_s = 320°, while during MY27 the green in the composite indicates it is brighter in L_s = 310°. These weekly changes are again in contrast with Figure 6 which indicates general stability from year-to-year. Also, while these sorts of variations are generally known in the literature, there is little work that has set out specifically to describe them, instead tending to focus on clouds surrounding the valley (e.g., Benson et al., 2003 who used MOC-WA; Clancy et al., 2009 used MARCI; and Leung et al., 2016 used HRSC).

2.9. Additional Variations

Figure 6, which shows RGB composites of different Mars Years at different L_s, provides the basis for this section. First, different panels within it have a different overall color cast, such as the top-right (L_s = 180°) being reddish overall. The overall cast indicates that Mars was brighter in that Mars Year (in that case, MY24), provided the caveat that there were no unaccounted-for gain changes in the instrument. Beyond what has been already discussed in this work, this section addresses four other areas of Mars; from West to East: A section of Amazonis Planitia, the margin between Chryse and Acidalia Planitias with Arabia Terra, the northern rim of Schiaparelli crater, and the margin between the Elysium Mons flanks and Utopia Planitia.

There is a linear, roughly horizontal (line of latitude) dark feature in Amazonis Planitia at ≈36–38°N, ≈195–205°E. South of this region is slightly lighter, but in Figure 6, the southern margin of it (≈30°N) appears multi-colored, indicating that there is significant brightness variation from year-to-year. Put another way, this albedo feature varies in extent from year-to-year. It is most clearly variegated for L_s = 0°, 60°, 120°, and 300°. However, for L_s = 300°, the variation is different, where the entire bright region below the dark feature (≈30–38°N) takes on the various hues, indicating differences from year-to-year.

The western margin of Arabia Terra, where it intersects with the Chryse and Acidalia planitias, also appears variegated in all L_s shown. It is rainbow, red to blue, from west to east, indicating that lighter material from Arabia Terra extended farther West in earlier years and it has moved East. Given the pixel scale of these data, the movement is roughly 15–20 km per year on average. However, Wellington & Bell (2020) briefly mention this boundary and note that they did *not* observe any shift with over a decade of the later MARCI data.

The large crater Schiaparelli is centered ≈–3°N, ≈17°E. Robbins (2020) noted that most craters had relatively stable reflectivity throughout the MOC-WA campaign (Hellas being a notable exception), though the rim of Schiaparelli was visible as a variable feature. Figure 6 emphasizes this variability for Schiaparelli's northern rim, which appears brightly hued in all six panels. In the left column, it appears cyan, while in the right column it appears more red. The cyan indicates that, between MY26–28, it was brighter in MY27 and 28 for those L_s; the red indicates that, for MY24 and MY26–27, it was brightest in MY24 for those L_s. Schiaparelli is an old crater, ~3.9 Ga (Robbins *et al.*, 2013), such that the rim and walls are practically non-existent. Therefore, this brightness extends into the crater floor for 10s km and then simply stops. There is no obvious topographic reason why this should be.

Finally, except for L_s = 180°, the western through northern margin of Elysium Mons' flanks appears variegated throughout the figure, indicating shifts of 10s km of the margins of bright material on the flanks versus dark material in the surrounding Utopia Planitia.

3. Exploring Changes in Mars' Atmosphere: North Polar Hood Formation

Discussed in the previous section, the NPH is a persistent cloud formation that covers much of Mars north of the arctic circle during its winter. It forms from the merger of other, more ephemeral clouds. How soon it forms has implications for atmospheric modeling which includes heat transfer and H_2O column density, so this investigation – while aimed towards showing the utility of this dataset – has broader science implications.

For this investigation, the $\Delta L_s = 5°$, then $\Delta L_s = 2°$ mosaics were examined. The longer averaging was used to initially narrow down when the NPH formed, while the shorter ones were used to pinpoint the transition to ≈4 days' fidelity. The color composites were used rather than blue-light mosaics because the more white cloud colorations stand out better than a blue brightness map. The $i \leq 90°$ mosaics were used because true brightness is unimportant for this exercise – only whether what types of clouds are visible – and the hood forms in twilight areas that would be masked by the $i \leq 75°$ cutoffs. A non-quantitative, visual inspection is the basis for this.

Using the criterion for when whiteish material mostly surrounds the north pole, the MOC-WA data show that in MY24, this occurs for $L_s \approx 160–162°$; for MY25, it occurs by $L_s \approx 158°–160°$; for MY26, it occurs by $L_s \approx 158°–162°$; and for MY27, it occurs by $L_s \approx 144°–146°$ (with full encircling by $L_s \approx 150°$. This early of a development is not previously reported in the literature, so far as we could tell, where Wang & Ingersoll (2002) reported $L_s \sim 160°–185°$ for MY24, and Calvin et al. (2015) reported $L_s \sim 158°$ in MY29 and MY30.

4. Exploring Changes in Mars' Dust Cover: Acidalia Planitia

Acidalia is a large, relatively flat, low-lying region in Mars' northern hemisphere, centered at ~50°N ~20°W. It has Tharsis to the west, Chryse to the south, and Arabia Terra to the southeast. North of it is Vastitas Borealis. It is a broad, dark feature unmatched in the northern hemisphere, and with dark regions south of it, it forms a practically continuous dark band from north to south across the planet. Therefore, when it fades or has portions that are interrupted, it is noticeable in a montage of the red mosaics or color composites. This has not been previously reported so far as we could (or, could not) find, and has implications for dust transport throughout the region.

For this investigation, the $\Delta L_s = 10°$ red mosaics for $i \leq 75°$ in equirectangular projection were used. This is a good mosaic set to use because the changes are to surface dust (best seen in red light), they are no where near the arctic circles (such that $i \leq 75°$ is sufficient), and the trend occurs over a longer period of time where the most accurate brightness is desired ($\Delta L_s = 10°$ is both desired and sufficient).

Acidalia is most distinct as an albedo feature during northern summer, and it is least distinct during southern summer. Indeed, in MY26 at $L_s = 320°$, as a dark feature, it has practically faded entirely, only to return to its previous darkness in MY27 during northern summer. This is reflected in Figure 7: Excluding MY25 where there was unexplained red gain sag ($L_s \sim 80$–$160°$) and a global dust storm, and excluding MY28 where there appears to be additional gain sag, Acidalia (Figure 7A) and Chryse (Figure 7B) show similar reflectivity between $L_s \sim 0$–$180°$. After that, Chryse remains a stable brightness, while Acidalia brightens, and it brightens in MY27 almost to the same reflectivity as Chryse. This is more easily seen in Figure 7C, which shows Acidalia relative to Chryse so removes any gain issues by treating Chryse as a control. Using the relative plot, MY25 and MY28 follow the pattern of other years despite the above-noted issues. The relative darkening of Acidalia during northern summer is fairly consistent, while the relative brightening is consistent as a phenomenon that occurs, but it is variable in its relative intensity.

5. Exploring Changes in Mars' Frost: Hellas Basin

Hellas is one of the lowest elevations on Mars, and as a large, mid-southern latitude feature, it can get cold enough that frost deposits will form every year. These deposits have been noted before, and even studied with the later MARCI camera (Calvin *et al.*, 2017). However, the seasonal deposition and sublimation of the frost, and any interannual variability, has not been studied with this dataset in this sort of detail.

For this investigation, the $\Delta L_s = 10°$ blue mosaics with $i \leq 90°$ were used. Blue light was used because the frost appears significantly brighter in blue than the surrounding dusty material, though the color composites could have been used and examined for white-appearing areas; similarly, a ratio of blue:red could be used. The $i \leq 90°$ were used because the frost develops and expands when some of the area of interest is in twilight, which would be eliminated if $i \leq 75°$ were used instead; however, one must be more cognizant of processing artifacts when using this cutoff. The equirectangular projection was used due to the simplicity of the projection, though the south polar projections would be a less distorted.

Initially, the approach was to map contiguous frost deposits manually in all $\Delta L_s = 10°$ mosaics; however, the frost is so bright compared to the dust in blue light that a reasonable automated thresholding could be used for the maps, instead, and then analyzed. Therefore, the region of Hellas and its immediate surroundings was examined, a small Gaussian blur applied to help reduce noise, and pixel values >0.075 were treated as having frost (*e.g.*, Figure 8A). Once the thresholding is done, one can simply count pixels and, scaling for cos(latitude), use the 9 ppd pixel scale to determine the area extent of frost as a function of time (Figure 8B).

The primary caveats to this method are two-fold. First, any thick, persistent clouds in the area will also be counted, but that should be minimal (Wang *et al*., 2011). Second is, if the frost is darker – or the gain in blue sagged and was not accounted for – then the thresholding would omit areas of frost since it is a simple cutoff. To mitigate this issue, a control region was selected to the northwest of Hellas' rim. The mean of the control region's values for the full time series were taken, the ratio of that overall mean vs. the mean of the control region at each time interval was multiplied into the brightness of the image, and *then* the thresholding was done.

To wit, if the threshold value of 7.5% were raised or lowered, it does raise or lower the amount of coverage in each image. This is unavoidable without, instead, performing detailed ice/frost mapping. However, the relative results do not change: Regardless of using a threshold of 0.05 or even 0.10, for example, there is less frost coverage in Hellas in MY25 than in other years at L_s = 85±5°. Similarly, it is found that there is less frost coverage at L_s = 135±5° in MY26 than in other years – due to the systematic shifting of MY26's data, Hellas' frost cover appears to both form and sublimate a few weeks earlier that year than during others (i.e., winter came and went a few weeks earlier that year), but the total frost cover during L_s = 100–120° is comparable to during other Mars Years. An additional feature visible in Figure 8B for all years is that there is an initial rapid growth of frost for about 40 Mars days, followed by slower growth until about L_s = 125±5°. After that point, the frost rapidly sublimates each year and is gone by L_s = 150°.

6. Summary and Discussion

The MOC-WA catalog of limb-to-limb images of Mars, taken from 1999 through most of 2006, is a significant resource in which NASA invested starting more than three decades ago. A newly processed version of the data provides a uniform, conveniently formatted archive of the entire time series in both red and blue light. The data have been demonstrated to reproduce well known features and trends about Mars, and the multi-dimensional dataset can be used for a myriad of other scientific investigations into Mars' surface and atmospheric processes during that four Mars Year time period.

This work also demonstrated additional changes on Mars through color composite analyses, primarily illustrating those that did not repeat annually, such as variations in ice extent at the poles and larger areas of relative brightening or darkening as seasons changed. In particular, the data were used here to perform investigations into the onset time of the North Polar Hood, the repeating variability in brightness of Acidalia, and the annual cycle of frost deposition and sublimation in Hellas.

The MOC-WA dataset is not widely used today, likely because it is considered older, worse quality than its successor, and it does not exist in an easy-to-use processed, archival form. It is hoped that this work, demonstrating its utility for new analyses, and the companion work (Robbins, 202X) that discusses the data processing, will show that useful information can still be gleaned from these older generation data. Combined with MARCI, they present an almost uninterrupted view of Mars from orbit spanning 1999 through the present day.

Acknowledgements: The author thanks B.J. Buratti and W.M. Grundy for useful discussions about photometric correction, T. Stryk for useful discussions about three-color composites from two colors, and T.M. Hare for innumerable emails about data repositories. The author acknowledges several hundred hours of "free time" in the preparation of this manuscript and dataset. The author acknowledges two anonymous reviewers and *JGR-P* Editor D. Rogers for helpful feedback on a previous version of this work.

Conflict of interest: The author declares no conflicts of interest relevant to this study.

Data Availability Statement: The MOC reflectivity maps used in this work are available from NASA's Imaging and Cartography Node (IMG) of the Planetary Data System (PDS) at Imaging and Cartography Node (https://ToBeFilledInIfAccepted).

Data Availability Statement for Manuscript Review: As noted in the front material, NASA's PDS "Imaging and Cartography" Node will be the final resting place for these data, which they have agreed to. The URL will be something close to: https://astrogeology.usgs.gov/search/map/Mars/GlobalSurveyor/MOC/Mars_Year24-28_MOCWAC_RedBlue_2022. Transferring the data to USGS will require shipping a hard drive and effort on USGS's part, though they have agreed to this. Because I do not want to burden them potentially multiple times, the intended PDS-like archive has been temporarily placed on my own server: http://www.sjrdesign.net/MOCWA. Please use this for evaluation purposes; any changes requested that are made will be to this preview version, and then that will be what is shipped to USGS for final archiving. Please also note that the uncompressed archive is ≈600 GB, so most folders have been compressed for download as single .ZIP files in this preview version.

References

(1895) Reports of the Mars Section. VI Syrtis Major. in Memoirs of the British Astronomical Association, 2, 182–189.

(1896) Report of the Mars Section. Solis Lacus and neighbouring region. in Memoirs of the British Astrnomical Association, 4, 112–113.

(1905) Opposition of 1896. From the Syrtis Major to the Indus. in Annals of the Lowell Observatory, 3, 1:55–1:62.

(1905) Opposition of 1903. Syrtis Major and its surroundings. in Annals of the Lowell Observatory, 3, 1:245–1:261.

(1927) Section for the Observation of Mars. 1919–1920. Section III. Solis Lacus. in Memoirs of the British Astronomical Association, 27, 18–20.

(1927) Section for the Observation of Mars. 1919–1920. Section VI. Syrtis Major. in Memoirs of the British Astronomical Association, 27, 29–34.

Benson, J. L., Bonev, B. P., James, P. B., Shan, K. J., Cantor, B. A., & Caplinger, M. A. (2003). The seasonal behavior of water ice clouds in the Tharsis and Valles Marineris regions of Mars: Mars Orbiter Camera Observations. Icarus, 165(1), 34–52. https://doi.org/10.1016/S0019-1035(03)00175-1

Benson, J. L., & James, P. B. (2003). Yearly comparisons of the Mars North Polar Cap: 1999, 2001, and 2003 MOC observations. in Third International Conference on Mars Polar Science and Exploration, Alberta, Canada. https://www.lpi.usra.edu/meetings/polar2003/pdf/8097.pdf

Benson, J. L., James, P. B., Cantor, B. A., & Remigio, R. (2006). Interannual variability of water ice clouds over major martian volcanoes observed by MOC. Icarus, 184(2), 365–371. https://10.1016/j.icarus.2006.03.014

Bonev, B. P., James, P. B., Bjorkman, J. E., & Wolff, M. J. (2002). Regression of the Mountains of Mitchel polar ice after the onset of a global dust storm on Mars. Geophysical Research Letters, 29(21). http://doi.org/10.1029/2002GL015458

Briggs, G. A., & Leovy, C. B. (1974). Mariner 9 observations of the Mars north polar hood. Bull. Amer. Met. Soc., 55, 278–296.

Byrne, S., Zuber, M. T., & Neumann, G. A. (2008).Interannual and seasonal behavior of Martian residual ice-cap albedo. Planetary and Space Science, 56(2), 194–211. https://doi.org/10.1016/j.pss.2006.03.018

Calvin, W. M., Cantor, B. A., & James, P. B. (2017) Interannual and seasonal changes in the south seasonal polar cap of Mars: Observations from MY 28–31 using MARCI. Icarus, 292, 144–153. https://doi.org/10.1016/j.icarus.2017.01.010

Calvin, W. M., James, P. B., Cantor, B. A., & Dixon, E. M. (2015) Interannual and seasonal changes in the north polar ice deposits of Mars: Observations from MY 29–31 using MARCI. Icarus, 251, 181–190. https://doi.org/10.1016/j.icarus.2014.08.026

Cantor, B. A. (2007). MOC observations of the 2001 Mars planet-circling dust storm. Icarus, 186(1), 60–96. https://10.1016/j.icarus.2006.08.019

Cantor, B. A., Malin, M., Edgett, K. S. (2002). Multiyear Mars Orbiter Camera (MOC) observations of repeated Martian weather phenomena during the northern summer season. Journal of Geophysical Research, 107(E3), CiteID 5014. https://doi.org/10.1029/2001JE001588

Cantor, B. A., James, P. B., & Calvin, W. M. (2010). MARCI and MOC observations of the atmosphere and surface cap in the north polar region of Mars. Icarus, 208, 61–81. http://doi.org/10.1016/j.icarus.2010.01.032

Cantor, B. A., Wolff, M. J., James, P. B., & Higgs, E. (1998) Regression of Martian north polar cap: 1990–1997 Hubble Space Telescope observations. Icarus, 136(2), 175–191. https://doi.org/10.1006/icar.1998.6020

Clancy, R. T., Grossman, A. W., Wolff, M. J., James, P. B., Rudy, D. J., Billawala, Y. N., et al. (1996). Water vapor saturation at low altitudes around Mars aphelion: A key to Mars climate? Icarus, 122(0108), 36–62. http://doi.org/10.1006/icar.1996.0108

Clancy, R. T., Montmessin, F., Benson, J., Daerden, F., Colaprete, A., & Wolff, M. J. (2017). Mars Clouds. In R. M. Haberle, R. T. Clancy, F. Forget, M. D. Smith, & R. W. Zurek (Eds.), The Atmosphere and Climate of Mars (pp. 76–105). chapter, Cambridge: Cambridge University Press. http://doi.org/10.1017/9781139060172.005

Clancy, R. T., Wolff, M. J., Cantor, B. A., Malin, M. C., & Michaels, T. I. (2009). Valles Marineris cloud trails. Journal of Geophysical Research, 114(E11), CiteID E11002. https://doi.org/10.1029/2008JE003323

Forget, F., Hourdin, F., Fournier, R., Hourdin, C., Talagrand, O., Collins, M., et al. (1999). Improved general circulation models of the Martian atmosphere from the surface to above 80 km. Journal of Geophysical Research, 104(E10), 24155–24175. http://doi.org/10.1029/1999JE001025

Geissler, P. E., & HiRISE Team (2012). Persistent surface changes in Solis Lacus, Mars. in Lunar and Planetary Science Conf. The Woodlands, TX https://www.lpi.usra.edu/meetings/lpsc2012/pdf/2598.pdf

Haberle, R. M., Clancy, R. T., Forget, F., Smith, M. D., & Zurek, R. W. (Eds.). (2017). The Atmosphere and Climate of Mars. Cambridge: Cambridge University Press. http://doi.org/10.1017/9781139060172

Hamilton, G. H. (1921). Changes in the Martian Syrtis Major opposition of 1920. Popular

Astronomy, 29, 73–76. https://articles.adsabs.harvard.edu/pdf/1921PA.....29...73H

Hernández-Bernal, J., Sánchez-Lavega, A., del Río-Gaztelurrutia, T., Ravanis, E., Cardesín-Moinelo, A., Connour, K., et al. (2021). An extremely elongated cloud over Arsia Mons volcano on Mars: I. Life cycle. Journal of Geophysical Research, 126, e2020JE006517. http://doi.org/10.1029/2020JE006517

Herschel, W. (1784) On the remarkable appearances at the polar regions of the planet Mars, the inclination of its poles, and its spheroidical figure; with a few hints relating to its real diameter and atmosphere. Philosophical Transactions of the Royal Society of London, 74, 233–273.

Huguenin, R. L. (1979). Mars: Remote sensing evidence for an oasis in the Solis Lacus region (–25°, 85°). in Press Abstracts: Lunar and Planetary Science Conference, Houston, TX https://articles.adsabs.harvard.edu/pdf/1979LPICo.363...30H

Iwasaki, K., Saito, Y., & Akabane, T. (1979). Behavior of the Martian north polar cap, 1975–1978. Journal of Geophysical Research, 84, 8311–8316. https://doi.org/10.1029/JB084iB14p08311

Iwasaki, K., Saito, Y., & Akabane, T. (1982). Martian north polar cap 1979–1980. in International Colloquium on Mars, Pasadena, CA. https://doi.org/10.1029/JB087iB12p10265

Iwasaki, K., Saito, Y., & Akabane, T. (1984). Martian north polar cap and haze 1981–1982. Astronomical Society of Japan, 36(2), 347–356. https://articles.adsabs.harvard.edu/pdf/1984PASJ...36..347I

Iwasaki, K., Parker, D. C., Larson, S., & Akabane, T. (1999). Martian north polar cap 1996–1997. Icarus, 138(1), 20–24. https://doi.org/10.1006/icaru.1998.6061

James, P. B. (1979). Recession of Martian north polar cap: 1977–1978 Viking observations. Journal of Geophysical Research, 84, 8332–8334. https://doi.org/10.1029/JB084iB14p08332

James, P. B. (1982). Recession of Martian north polar cap: 1979–1980 Viking observations. Icarus, 52(3), 565–569. https://doi.org/10.1016/0019-1035(82)90016-1

James, P. B., Briggs, G., Barnes, J., & Spruck, A. (1979). Seasonal recession of Mars' south polar caps as seen by Viking. Journal of Geophysical Research, 84, 2889–2922. https://doi.org/10.1029/JB084iB06p02889

James, P. B., & Cantor, B. A. (2001). Martian north polar cap recession: 2000 Mars Orbiter Camera Observations. Icarus, 154(1), 131–144. https://doi.org/10.1006/icaru.2001.6653

James, P. B., & Cantor, B. A. (2002). Atmospheric monitoring of Mars by the Mars Orbiter Camera on Mars Global Surveyor. Advances in Space Research, 29(2), 121–129. https://doi.org/10.1016/S0273-1177(01)00561-0

James, P. B., Cantor, B. A., & Davis, S. (2001). Mars Orbiter Camera observations of the Martian south polar cap in 1999–2000. Journal of Geophysical Research, 106(E10), 23635–23652. https://doi.org/10.1029/2000JE001313

Leung, C. W. S., Rafkin, S. C. R., Stillman, D. E., & McEwen, A. S. (2016). Fogs and Clouds are a potential indicator of a local water source in Valles Marineris. in Lunar and Planetary Science Conference, The Woodlands, TX. https://www.hou.usra.edu/meetings/lpsc2016/pdf/2878.pdf

Lee, S. W. (1986). Regional sources and sinks of dust on Mars: Viking observations of Cerberus, Solis Planum, and Syrtis Major. in Symposium on Mars: Evolution of its Climate and Atmosphere, Washington, D.C. https://articles.adsabs.harvard.edu/pdf/1986LPICo.599...57L

Malin, M. C., Danielson, G. E., Ravine, M. A., & Soulanille, T. A. (1991). Design and development of the Mars observer camera. International Journal of Imaging Systems and Technology, 3(2), 76–91. http://doi.org/10.1002/ima.1850030205

Millour, E., Forget, F., Spiga, A., Vals, M., Zakharov, V., Montabone, L., et al. (2018). The Mars Climate Database. Presented at From Mars Express to ExoMars, Madrid, Spain, 27–28 February 2018.

Mitchel, O. M., Observations of Mars, Sidereal Messenger, 2, 101, 1846.

Mouginis-Mark, P. J., Cintala, M. J., & Whitford-Stark, J. L. (1980). Geological constraints for the Solis Planum "oasis" on Mars. in Lunar and Planetary Science Conference, Houston, TX. https://articles.adsabs.harvard.edu/pdf/1980LPI....11..762M

O'Leary, B., & Jackel, L. (1970). The 1969 opposition effect of Mars. Full disk, Syrtis Major and Arabia. Icarus, 13(3), 437–448. https://doi.org/10.1016/0019-1035(70)90091-6

Read, P. L., Collins, M., Forget, F., Fournier, R., Hourdin, F., Lewis, S. R., et al. (1997). A GCM climate database for Mars: For mission planning and for scientific studies. Advances in Space Research, 19(8), 1213–1222. http://doi.org/10.1016/S0273-1177(97)00272-X

Robbins, S. J., Hynek, B. M., Lillis, R. J., & Bottke, W. F. (2013). Large impact crater histories of Mars: The effect of different model crater age techniques. Icarus, 225, 173–184. http://doi.org/10.1016/j.icarus/2013.03.019

Robbins, S. J. (2020). Mars's Red (575–625 nm) seasonal approximate reflectivity averaged over Mars Years 24–28 from Mars Orbiter Camera. Journal of Geophysical Research, 125, e2019JE006231. http://doi.org/10.1029/2019JE006231

Robbins, S. J. (2021). Mars Orbiter Camera Red and Blue Global Mosaics for 1999 through 2006 (Version 1.0.0) [Data set]. Zenodo. http://doi.org/10.5281/zenodo.5526893

Robbins, S. J. (202X). Mars Global Surveyor's Mars Orbiter Camera (MOC) Wide-Angle Images (1999–2006): 1. Data Processing. submitted to Earth & Space Science concurrently with this manuscript as a companion

Robbins, S. J. (202X). Mars Orbiter Camera Red and Blue Global Mosaics for 1999 through 2006 (Version 1.0.0) [Data set]. NASA PDS. https://ToBeFilledInIfAccepted

Slipher, E. C. (1921) Obscuration of the Martian Syrtis Major. Popular Astronomy, 29, 66–73. https://articles.adsabs.harvard.edu/pdf/1921PA.....29...69S

Slipher, E. C. (1962) The Photographic Story of Mars. Sky Publishing Corp., Cambridge, MA.

Soderblom, L. A., Malin, M. C., Cutts, J. A., & Murray, B. C. (1973). Mariner 9 observations of the surface of Mars in the north polar region. Journal of Geophysical Research, 78(20), 4197–4210. https://doi.org/10.1029/JB078i020p04197

Thompson, D. T. (1972). The variation in contrast of Syrtis Major in 1971. Bulletin of the American Astronomical Society, 4, 313.

Wang, H., & Ingersoll, A. P. (2002). Martian clouds observed by the Mars Global Surveyor Mars Orbiter Camera. Journal of Geophysical Research, 107(E10:5078), 8pp. http://doi.org/10.1029/2001JE001815

Wang, H., & Richardson, M. I. (2015). The origin, evolution, and trajectory of large dust storms on Mars during Mars years 24–30 (1999–2011). Icarus, 251, 112–127. https://doi.org/10.1016/j.icarus.2013.10.033

Wang, H., Toigo, A. D., & Richardson, M. I. (2011). Curvilinear features in the southern hemisphere observed by Mars Global Surveyor Mars Orbiter Camera. Icarus, 2015(1), 242–252. https://doi.org/10.1016/j.icarus.2011.06.029

Wellington, D. F., & Bell, J. F. (2020). Patterns of surface albedo changes from Mars Reconnaissance Orbiter Mars Color Imager (MARCI) observations. Icarus, 239(113766). http://doi.org/10.1016/j.icarus.2020.113766

Zinzi, A., Palomba, E., & D'Amore, M. (2006). Monitoring albedo variations on Syrtis Major region of Mars from 1999 to 2004. in European Planetary Science Congress, Berlin, Germany. https://articles.adsabs.harvard.edu/pdf/2006epsc.conf...95Z

SEE SEPARATE UPLOAD DUE TO FILE SIZE

Figure 1. Basemaps are an average, in order, of L_s = 0°, 180°, 90°, and 270° (each ±5°, and the averages are from MY24–28). Top two panels are equirectangular projections, bottom two are north (left) and south (right) polar stereographic. Top— Nomenclature map for each feature discussed in the text. Larger font size indicates larger features (*e.g.*, Tharsis covers ≈25% of Mars). Other— Graticule guide in the different projections. [© Note: This identical figure is used in the companion paper.]

Note for Reviewers/Editors/Typesetters: Figure should be full-page width, color.

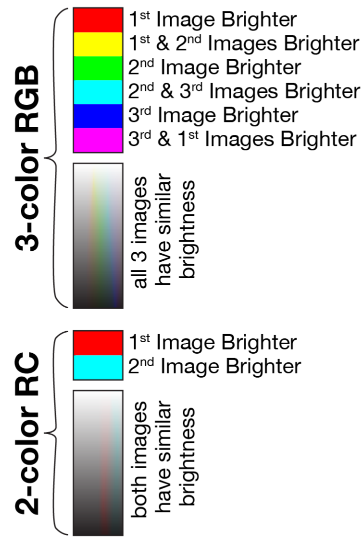

Figure 2. Red-green-blue and red-cyan color scale bars. Note that approximately equal brightness in each band will still show a slight color, so significance is only derived when there is a substantial difference, seen as a significant color saturation.

Note for Reviewers/Editors/Typesetters: Figure should be third-page width, color.

SEE SEPARATE UPLOAD DUE TO FILE SIZE

Figure 3. RC composite showing Mars before versus after the 2001 dust storm. See Figure 2 for color scale interpretation. The significantly redder bands at southern latitudes indicate $L_s = 180°$ was brighter there, which is due to seasonal frost that sublimated by $L_s = 270°$.

Note for Reviewers/Editors/Typesetters: Figure should be full-page width, color.

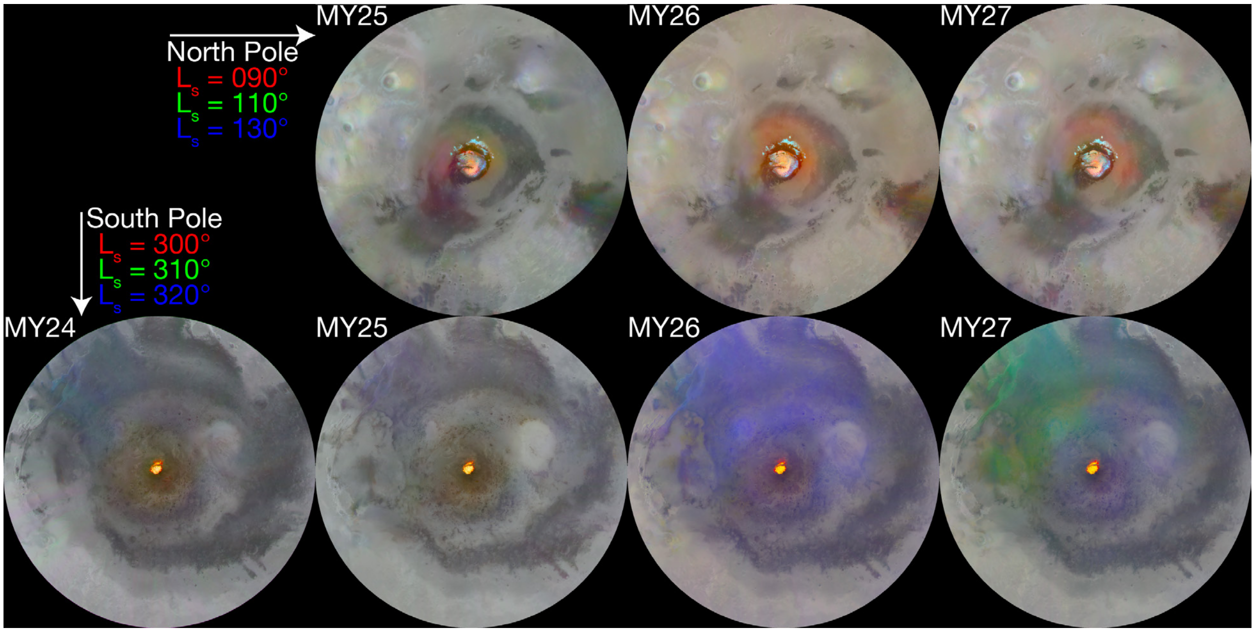

Figure 4. North (top row) and South (bottom row) polar projections showing changes in the residual polar ice caps and surrounding terrain as the seasons progress past each solstice for different Mars Years. Images are an RGB composite of MOC-WA red filter mosaics. See Figure 2 for color scale interpretation.

Note for Reviewers/Editors/Typesetters: Figure should be full-page width, color.

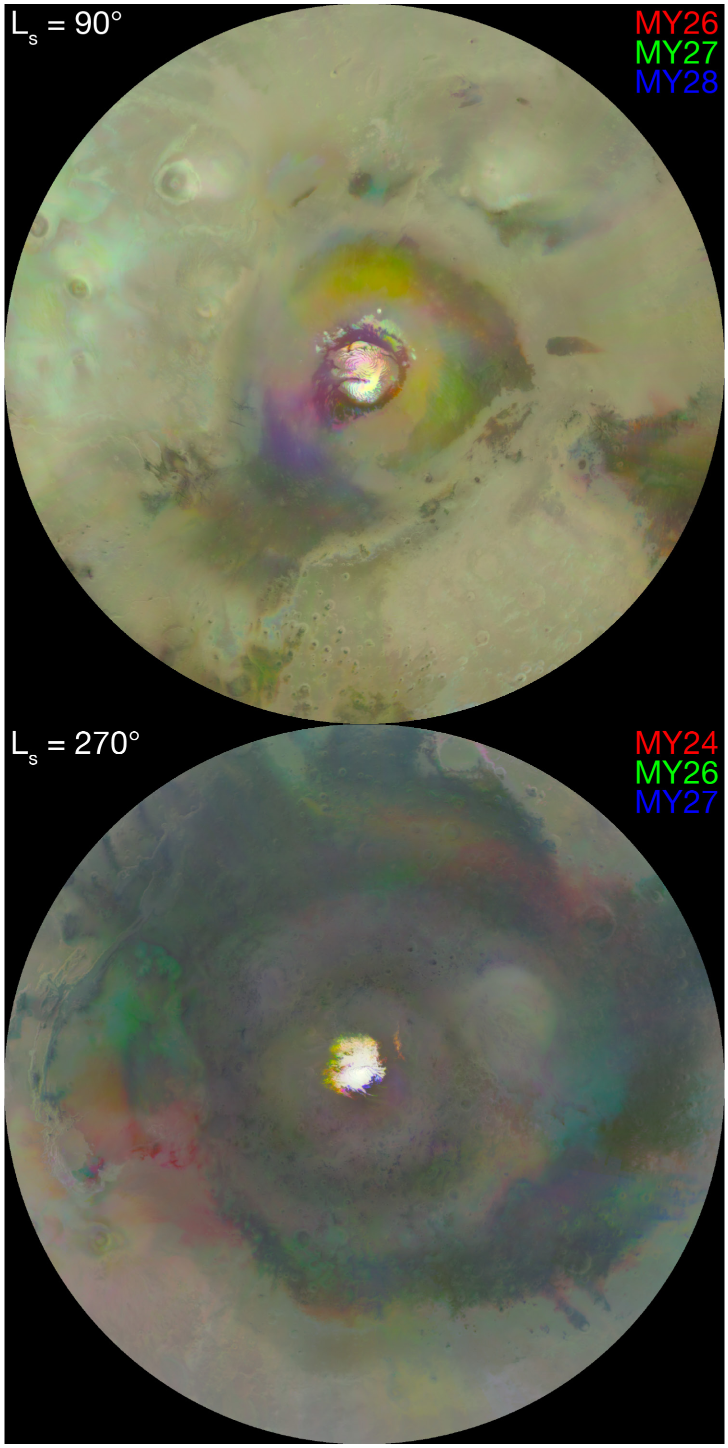

Figure 5. North (top) and South (bottom) polar projections showing changes in the residual polar ice caps and surrounding terrain as the Mars Year changes. Images are an RGB composite of MOC-WA red filter mosaics (see Figure 2 for color scale interpretation). Despite having four years of data at each L_s, only three are shown because of the color composite method. MY25

was omitted from the north because of the gain sag discussed in the text, and it was omitted from the south because it was an abnormal year with a global dust storm.

Note for Reviewers/Editors/Typesetters: Figure should be third-page width, color.

SEE SEPARATE UPLOAD DUE TO FILE SIZE

Figure 6. RGB composites of three Mars Years at six L_s, evenly spaced by 60° of L_s, using MOC-WA red filter data (see Figure 2 for color scale interpretation). MY25 was avoided for L_s = 0–120° due to known gain issues, while MY25 was avoided for L_s = 180–300° due to the global dust storm. The MOC-WA blue camera was not used due to issues processing MY27 data, and the purpose of this Figure is to illustrate surface rather than cloud differences.

Note for Reviewers/Editors/Typesetters: Figure should be full-page width, color.

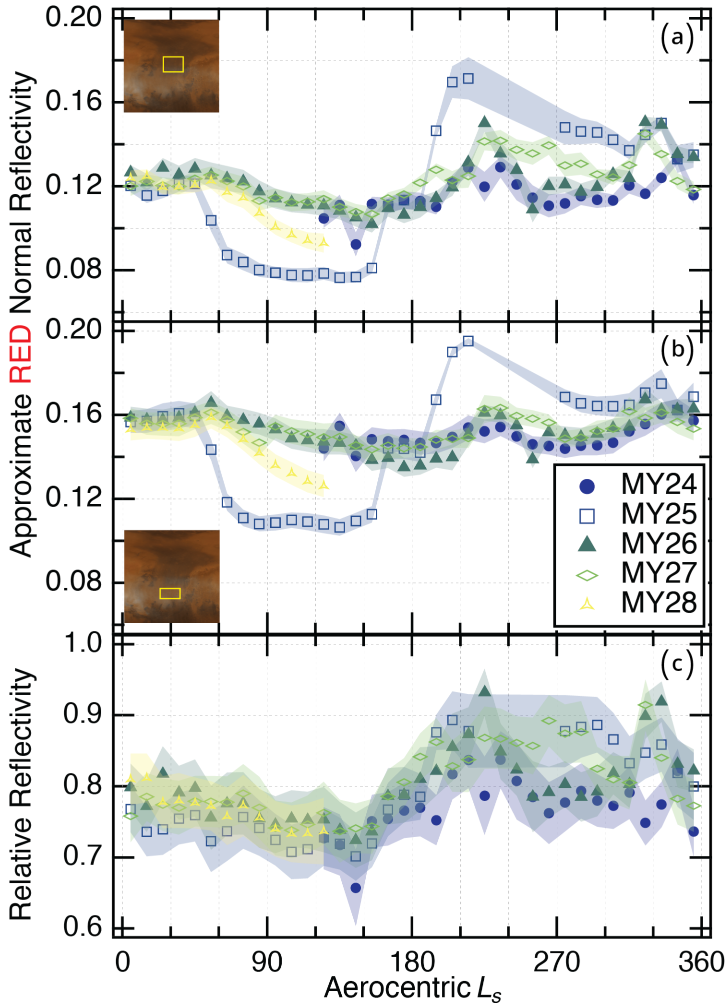

Figure 7. Periodic variation in red reflectivity of Acidalia Planitia (A) compared with Chryse Planitia (B), with each datum being the average of pixel values in the yellow boxes. Panel (C) shows the top divided by the middle to show relative variation, treating Chryse as a control. Error bands in the top and middle panel reflect standard deviations within each region, bottom panel bands used standard propagation of uncertainty methods.

Note for Reviewers/Editors/Typesetters: Figure should be half-page width, color.

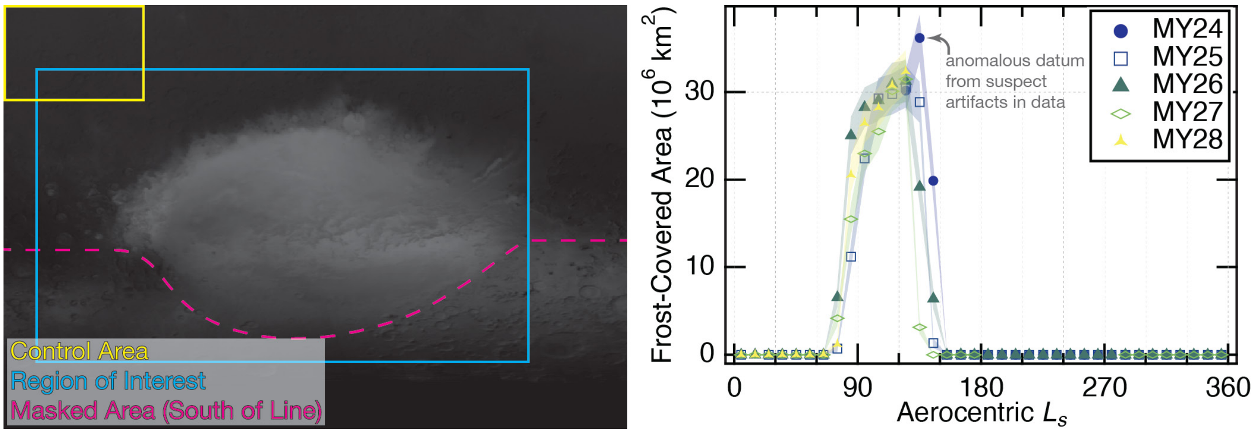

Figure 8. Hellas crater frost analysis in blue light. The left panel shows the region of interest along with the area that were masked from analysis and the area to the northwest that was used as a gain control. The right panel shows the results as an area of frost coverage when using brightness values >7.5% reflectivity in the blue data.

Note for Reviewers/Editors/Typesetters: Figure should be full-page width, color.